Received: 17 January 2022 | Revised: 1 April 2022 | Accepted: 13 May 2022

DOI: 10.1002/aic.17761

AIChE JOURNAL

RESEARCH ARTICLE

Process Systems Engineering

AI models for correlation of physical properties in system of 1DMA2P-CO_2-H_2O

Helei Liu[1,2,3] | Xiaotong Jiang[1] | Raphael Idem[2] | Shoulong Dong[1] | Paitoon Tontiwachwuthikul[2]

[1]International Innovation Institute of Carbon Capture and Utilization (I3CCU), School of Chemistry and Chemical Engineering, Beijing Institute of Technology, Beijing, China

[2]The Clean Energy Technologies Research Institute (CETRI), University of Regina, Regina, Saskatchewan, Canada

[3]Department of Chemical and Biological Engineering, The University of British Columbia, Vancouver, British Columbia, Canada

Correspondence
Helei Liu and Shoulong Dong, International Innovation Institute of Carbon Capture and Utilization (I3CCU), School of Chemistry and Chemical Engineering, Beijing Institute of Technology, Beijing 102488, China.
Email: lhl0925@hotmail.com, hl_liu@bit.edu.cn and sldong@bit.edu.cn

Raphael Idem, The Clean Energy Technologies Research Institute (CETRI), University of Regina 3737 Wascana Parkway, Regina, Saskatchewan S4S 0A2, Canada
Email: raphael.idem@uregina.ca

Funding information
Beijing Institute of Technology; Natural Science and Engineering Research Council of Canada (NSERC)

Abstract

In this work, the density, viscosity, and specific heat capacity of pure 1-dimethylamino-2-propanol (1DMA2P) as well as aqueous unloaded and CO_2-loaded 1DMA2P solution (with a CO_2 loading of 0.04–0.70 mol CO_2/mol amine) were measured over the 1DMA2P concentration range of 0.5–3.0 mol/L and temperature range of 293–323 K. The observed experimental results of these thermophysical properties of the 1DMA2P-H_2O-CO_2 system were correlated using empirical models as well as artificial neural network (ANN) models (namely, back-propagation neural network [BPNN] and radial basis function neural network [RBFNN] models). It was found that the developed BPNN and RBFNN models could predict the experimental results of 1DMA2P-H_2O-CO_2 better than correlations using empirical models. The results could be treated as one of the accurate and potential methods to predict the physical properties for aqueous amine CO_2 absorption systems.

KEYWORDS
1DMA2P, ANN models, CO_2 loading, empirical model, physical properties

1 | INTRODUCTION

The current climate crisis, one of greatest challenges of our times, has drawn considerable international effort to address and tackle the issue. The 26th Conference of the Parties (COP26) of the United Nations Framework Convention on Climate Change has indicated that strengthening of global collaboration and action on greenhouse gas emissions must be put into force based on the foundation of the 2015 Paris Agreement.[1] An increasing number of countries have announced the net zero pledges by 2050 to reduce carbon dioxide emissions to net zero and to limit the long-term increase in average global temperature to 1.5°C. Carbon capture, utilization and storage from fossil fuel has commonly been considered to play an increasingly significant role in reducing CO_2 emissions, especially in power stations and heavy industries such as steel, cement, and chemicals.[2] Direct air capture with carbon capture and storage also provides the potential for eliminating carbon emissions.[3] In addition, the deployment of bioenergy with carbon capture and storage could also provide the potential technology for negative carbon emissions to accelerate the process of net zero carbon emissions.[4] As one of the main carbon capture technologies, post-combustion carbon capture (PCCC) from flue gases generated from fossil fuel power plants is vital for deployment to mitigate CO_2 emissions since PCCC could easily be integrated and implemented into both existing and new industrial plants (i.e., cement plants, steel plants, etc.) and power stations such as natural gas-fired power stations.[5] Meanwhile, PCCC could offer a lower technology

risk and a higher operational flexibility in comparison with other competing technologies.[6] PCCC with chemical absorption based mainly on amines has been considered to be a commercially feasible as well as most suitable way to treat large volumes of flue gases containing low concentrations of CO_2 due to its advantages of high reactivity and high absorption capacity.[7] However, this PCCC technology based on amines suffers from some critical disadvantages of high energy requirements for amine regeneration and amine degradation.[8]

Some researchers contribute to improving the performance of amine-based solvents by using blends scrubbing system,[9] shifting from aqueous to water lean solvents,[10] while others focus on screening alternatives to the traditional amines.[11,12] One of that can help to address the issue of energy consumption is to develop efficient amine solvents with high capacity, fast absorption rate, and low heat duty.[13] Thus, researchers are putting in a lot of efforts in formulating the efficient solvents for next generation of CO_2 capture. Luo et al.[14] worked on two unique molecules absorbents of 4-(2-hydroxyethylamino) piperidine (A4) and 1-(2-hydroxyethyl)-4-aminopiperidine (C4) with respect to solubility and cyclic loading, which exhibited a better CO_2 capture performance in comparison with typical amines such as monoethanolamine (MEA), 2-([2-aminoethyl]amino)ethanol (AEEA), etc. In the work of Yu et al.,[15] three diamines of 1,3-PDA, DMAPA, and MAPA among the nine studied diamines gave a faster absorption rate and higher mass transfer coefficient. As presented in the work of Zheng et al.,[16] N-(2-hydroxyethyl) pyrrolidine also showed a high application potential with a higher CO_2 capacity. Recently, 1-dimethylamino-2-propanol (1DMA2P), a new tertiary amine has been drawing considerable attention due to its favorable performance in amine-based PCCC. Kadiwala et al.[17] investigated 1DMA2P solution using a stopped-flow apparatus and found that 1DMA2P could react faster with CO_2 than MDEA. Chowdhury et al.[18] presented that 1DMA2P possessed much higher CO_2 cyclic capacities and absorption rates than those of MDEA. Liang et al.[19] reported that 1DMA2P showed much better mass transfer performance than MDEA. Liu et al.[20,21] proved that 1DMA2P had preferable CO_2 equilibrium solubility and diffusivity performance. All the merits provide a high potential for industrial applications.

As was pointed out, a comprehensive study of this solvent (e.g., mass transfer, thermodynamic characteristics, and heat duty) should be conducted before its commercial application.[22] Physicochemical properties of solvents such as density, viscosity, and specific heat capacity are regarded as some of the important parameters employed for practical application. In addition, those physical properties are necessarily required for the determination of the reaction kinetics model as well as the design of gas–liquid contactor columns since densities and viscosities data are essential for their calculations.[22] Those data could be used for determining the column diameter, velocities, and pressure drop in the column as described by Eckert[23] as well as the calculation of mass transfer correlations and mass transfer area as described by Wang et al.[24] In addition, density and viscosity have a significant effect on the mass transfer coefficient, hydrodynamic behavior, and diffusivity behavior. Both density and viscosity are necessary for the design of the absorber and stripper column.[25] Another physical property, specific heat capacity, represents the required amount of heat to change the temperature of a specific amount of a substance to a certain temperature. The specific heat capacity of a system could be presented as the ratio of the heat that should be added or withdrawn to/from the system to change the temperature. The specific heat capacity of amine solvent is required for heat exchanger design for the CO_2 capture plant. Meanwhile, the experimental data of physical properties of unloaded 1DMA2P and loaded 1DMA2P are not available in the literature.

In this work, the densities and viscosities of pure 1DMA2P were measured over the temperature of 293–323 K. The specific heat capacity of pure 1DMA2P was measured over the temperature range of 298–323 K. In addition, the density data and viscosity of 1DMA2P solution with different concentration were also measured over the 1DMA2P concentration range of 0.5–3.0 mol/L and temperature range of 293–323 K. Densities and viscosities of loaded 1DMA2P were also obtained in this work at the CO_2 loading range of 0.04–0.7 mol CO_2/mol amine, concentration range of 0.5–3.0 mol/L, and temperature range of 293–323 K. The specific heat capacity of 1DMA2P solution was also measured over the concentration of 0.5–3.0 mol/L and temperature range of 298–323 K. The specific heat capacity of loaded 1DMA2P solution was also obtained at the CO_2 loading range of 0.04–0.7 mol CO_2/mol amine, concentration range of 0.5–3.0 mol/L, and temperature range of 298–323 K. Some models were employed to correlate and predict these physical properties of the 1DMA2P-H_2O-CO_2 systems. Artificial neural network (ANN) models were also developed to predict the experimental results of 1DMA2P physical properties.

2 | EXPERIMENTAL SECTION

2.1 | Chemical

Reagent grade 1DMA2P with a purity of ≥99 wt.% was obtained from Sigma-Aldrich. The amine solutions were prepared to the desired concentrations using deionized water. Carbon dioxide (CO_2) gas with purity of 99.9% was obtained from Praxair Inc. The CO_2-loaded solutions were prepared via a CO_2 absorption apparatus described in our previous work,[19] which was made up of five parts, namely a CO_2 cylinder, mass flow meter, dryer, saturator, and a three-necked flask reactor. Every 5 min, a 2 ml solution sample was taken to analyze CO_2 loading (α) which was measured by titration with a Chittick CO_2 analyzer.

2.2 | Density

Densities were measured using a density meter of model DMA 4500M (Anton Paar) with an accuracy of 0.00001 g/cm^3. The temperature of the system was controlled within an accuracy of 0.01 K. Before the measurement of density, the density meter was cleaned using acetone and methanol, and then well dried with air. After that, the sample was injected to measure the density. All the process (i.e., cleaning, drying, injection, and measurement) were conducted automatically. In order to obtain reliable results, all the samples were run two times and the average was achieved for the final result. The equipment was calibrated by measuring the density of 5 mol/L MEA over the temperature range of 298–333 K. The

results are shown in Figure 1. It was found that the measured densities of 5 mol/L MEA are consistent with those from the reference with an absolute average deviation (AAD) of 0.04%. It was confirmed that the results observed from this work are reliable.

2.3 | Viscometer

The viscosity data were obtained by using Lovis viscometer (Anton Paar) with an accuracy of 0.5%. The temperature of the system was controlled with an accuracy of 0.01 K as well. As in the case of density meter, the system was cleaned using the acetone and methanol and was dried by air, and then introduced to DMA 4500M and Lovis 2000 at the same time. The viscosity was measured at the desired temperature. The result of viscosity of the sample is given as an average of two measurements. In order to calibrate the viscometer, the viscosity of 5 mol/L MEA was measured to compare to the values from Reference 26. As shown in Figure 2, it was found that the obtained results in this work agreed very well with the values from literature. It was confirmed that the results observed from this work are reliable.

2.4 | Thermal conductivity meter

The measurements of thermal conductivity, thermal diffusivity, and specific heat capacity were by obtained by employing thermal

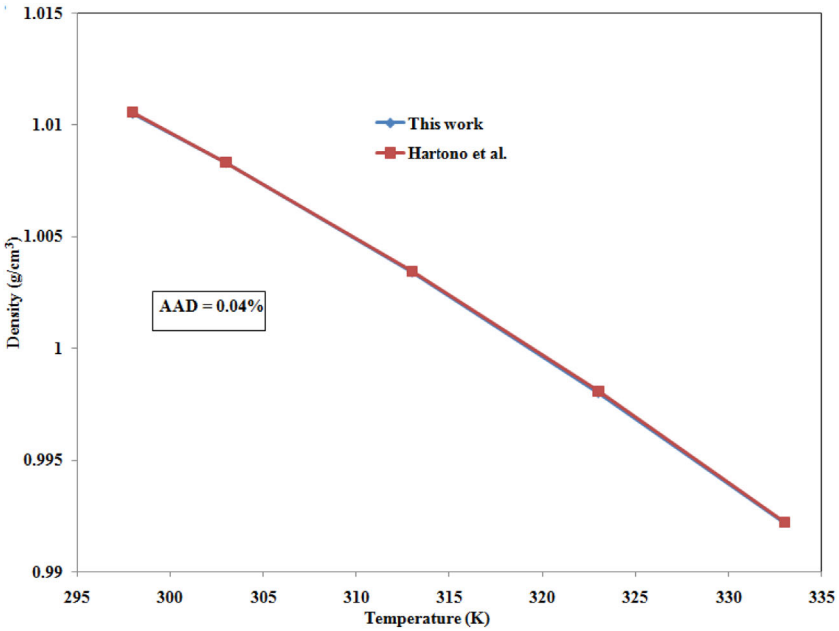

FIGURE 1 Validation of density meter using the density of 5 mol/L monoethanolamine (MEA) from Reference 26

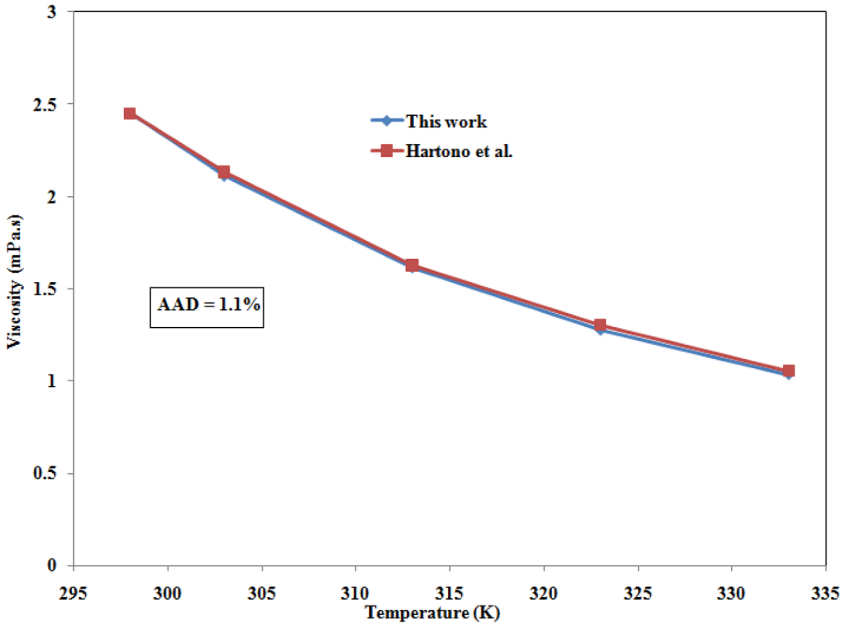

FIGURE 2 Validation of viscometer using the viscosity of 5 mol/L monoethanolamine (MEA) from Reference 26

conductivity meter (THW-LAMBDA). This performance of thermal conductivity meter was achieved using a transient. Firstly, the liquid sample was introduced into the stainless steel bottle. And then, a thin wire was fitted to the bottle and immersed into the sample. A current was passed through the wire in order to heat the sample. The resistance as a function of time was obtained. Meanwhile, the temperature of sample was also monitored. Thermal properties of a sample can be automatically generated based on the typical graph of current versus time using THW-LAMBDA, which gives an accuracy of 5%. Three measurements of each sample were obtained in order get the average value. A validation of the thermal conductivity meter was performed by measuring the specific heat capacity of pure water. It was found that results measured in this work are reliable.

3 | RESULTS AND DISCUSSIONS

As is well known, the solvent used in the CO_2 capture plan is cycled between the absorber and stripper to respectively absorb and release CO_2. The loaded amine solution and the unloaded solution is used in this way during practical application. Therefore, the physical properties of amine solution under different conditions are essential for the operation of a CO_2 capture process.

3.1 | Density

Densities of pure 1DMA2P were measured over the temperature range of 293–323 K, which are shown in Table 1 and Figure 3. From Figure 3 and Table 1, it can be seen that the density decreased as the increase of temperature. This is because an increase in temperature leads to volume expansion of the solution, which leads to a decrease in density. In order to correlate the experimental data, some correlations were employed to fit the obtained results. In this work, linear and nonlinear fittings were used to fit the density values of pure 1DMA2P. All the results are shown in Figures 3 and 4. From Figures 3 and 4, it can be seen that both linear and nonlinear equations could represent the experimental results very well. The fitting linear and nonlinear equations are given in the following equations:

$$\text{Linear equation}: D = A \times T + B \quad (1)$$

$$\text{Nonliner equation}: D = C \times \text{Exp}\left(\frac{E}{T}\right) \quad (2)$$

The values of the coefficients were obtained by fitting the measured data to Equations (1) and (2), respectively. All the obtained results are shown in Table 2.

From Figures 3 and 4, it could be seen that both the linear and nonlinear fittings could correlate the experimental data very well. However, the linear equation appears to represent the results a bit better than the nonlinear equation. Thus, the linear equation was used to correlate the density results of 1DMA2P solution.

The density of unloaded 1DMA2P solution was measured over the concentration of 0.5–3 mol/L and the temperature range of 293–323 K. All the results are shown in Figure 5. As shown in Figure 5, the density exhibited an increasing trend as a function of temperature for all different concentrations system. From Figure 5, it

TABLE 1 Density of pure 1-dimethylamino-2-propanol (1DMA2P) as function of temperature

T (K)	Density (g/cm^3)
293.01	0.84946
297.99	0.84470
302.99	0.83990
307.99	0.83508
312.99	0.83023
318.01	0.82536
322.99	0.82047

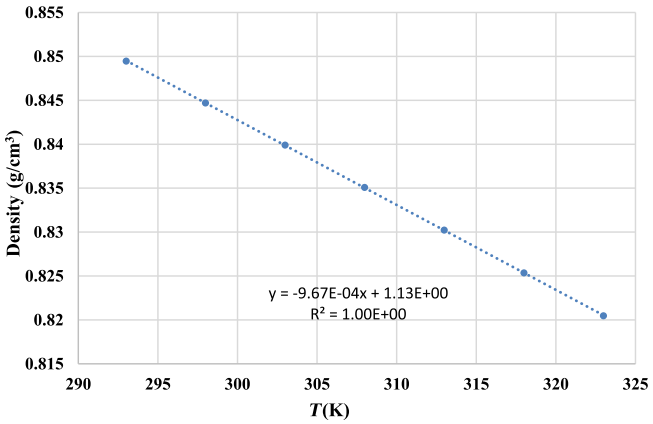

FIGURE 3 Effect of temperature on the density of the pure 1-dimethylamino-2-propanol (1DMA2P)

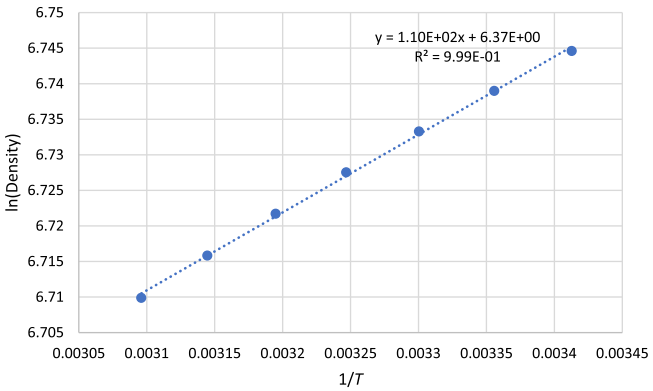

FIGURE 4 Effect of temperature on the density of the pure 1-dimethylamino-2-propanol (1DMA2P)

can be seen that the density decreased with an increase in concentration at the same temperature. This is because the density of water is higher than that of 1DMA2P. The more the ratio of water in the solution, the higher will be the density of the resulting 1DMA2P solution. The liner equation (Equation 1) was used to correlate the experimental results as shown in Figure 5. From Figure 5, it was found that the linear equation could correlate the experimental density of 1DMA2P solution very well. All the coefficients of *A* and *B* of Equation (1) were obtained by using this linear fitting. These are shown in Table 3. As shown in Table 3, the values of *B* for different concentration are very close without a big difference, which could be considered as one value. From Equation (1) and Figure 5, *B* represents the intercept. It means the density of the system at the temperature of 0 K, which is impossible to reach. At this point, the 1DMA2P solution with different concentration may be the same status, which may give the same value of density. Because, there are only molecules of water and 1DMA2P in all the systems. This is why the values of *B* for different systems are almost the same. In order to get the general value of *B*, the average of *B* (B_1) for different concentration was calculated as 1.14. Values of *A* were fitted to the following equation:

$$A = A_1C^2 + A_2C + A_3 \tag{3}$$

where *C* is the concentration.

The coefficients of A_1, A_2 and A_3 were obtained, which were shown in Table 4. The general equation used to predicate the density of 1DMA2P solution could be expressed as in Equation (4):

$$D = \left(A_1C^2 + A_2C + A_3\right)T + B_1 \tag{4}$$

All the calculated coefficients are shown in Table 4. This equation can be used to represent the density of 1DMA2P solution. The calculated results of density were compared with the experimental results. It was observed that the predicated results have good agreement with the experimental data with an absolute deviation of 2.3%.

In addition, densities of 1DMA2P solution loaded with CO_2 were measured over the concentration of 0.5–3.0 mol/L and the temperature range of 293–323 K. All the results are shown in Figures S1–S5 in Supplemental Materials. From these figures, the density exhibited a decreasing trend as the temperature was increased, and an increasing trend as the CO_2 loading was increased. As a result of the addition of

TABLE 2 Values of coefficients

Coefficients	Values	Coefficients	Values
A	−9.67E-04	*C*	1.10E+02
B	1.13	*E*	6.37

TABLE 3 Coefficients of *A* and *B* for different concentration

Concentration (mol/L)	*A*	*B*
0.5	−4.16E-04	1.12
1.0	−4.09E-04	1.11
1.5	−4.52E-04	1.13
2.0	−5.35E-04	1.15
3.0	−6.84E-04	1.19

TABLE 4 Coefficients of the general equation

Coefficients	Values
A_1	−3.93E-05
A_2	2.47E-05
A_3	−4.09E-04
B_1	1.14

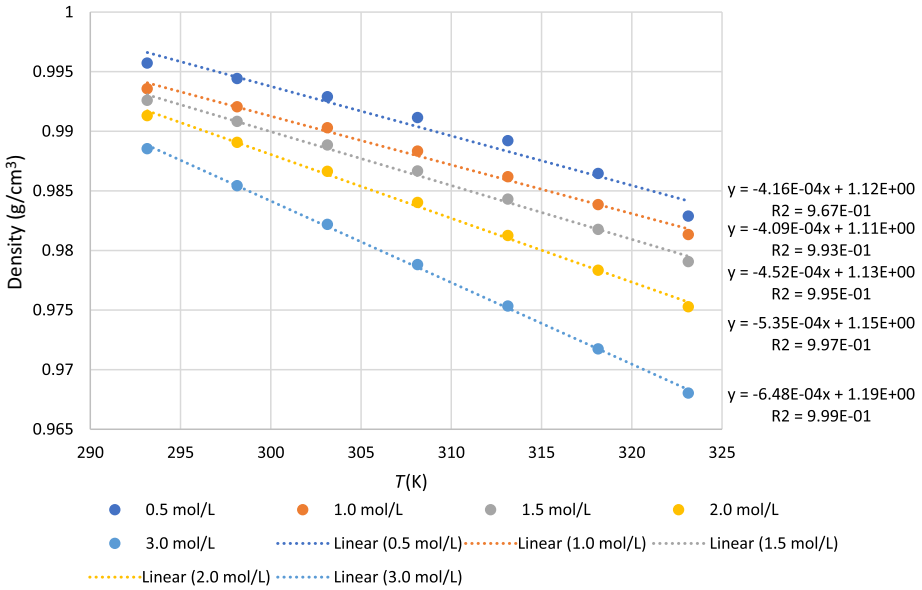

FIGURE 5 Effect of concentration and temperature on the density of 1-dimethylamino-2-propanol (1DMA2P) solution

CO_2 in the solution, the weight of system increased which resulted in the increase of density. In order to correlate the density of loaded 1DMA2P solution, Equation (1) was used to fit the experimental results, which are presented in Figures S1–S5. The value of *B* for each loaded 1DMA2P solution was obtained similar to the system of unloaded 1DMA2P, as shown in Table 5. The general value of *B* for loaded 1DMA2P solution (B_1) could be obtained by calculating the average of all the values of *B* for all systems, which is estimated to be 1.17. The values of *A* for different concentrations as a function of CO_2 loading are shown in Table 6. The values of *A* for different systems were plotted as function of CO_2 loading, and then fitted to the following equation as:

$$A = A_1\alpha^2 + A_2\alpha + A_3 \tag{5}$$

where α is CO_2 loading.

All the coefficients of A_1, A_2, and A_3 are shown in Table 7.

It can be seen in Table 7 that A_1, A_2 and A_3 have a relationship with concentration. In order to find out the relationship of concentration and coefficients A_i, the A_i was plotted as a function of the concentration. The fitting equation is shown in Equation (6):

$$A_i = B_1C^2 + B_2C + B_3 \tag{6}$$

All the coefficients are shown in Table 8. By using all obtained values, the densities of loaded 1DMA2P solution were represented. The calculated results of density were then compared with the experimental results. It was observed that the predicated results have good agreement with experimental results with an AAD of 4.0%.

TABLE 5 Values of *B* for different concentration loaded 1-dimethylamino-2-propanol (1DMA2P) solution

Concentration (mol/L)	*B*
0.5	1.12
1.0	1.14
1.5	1.16
2.0	1.19
3.0	1.25

3.2 | Viscosity

Viscosities of pure 1DMA2P were measured over the temperature range of 293–323 K. These are shown in Table 9 and Figure 6. From the figure and table, it can be seen that the viscosity decreased as the temperature was increased. It is because that the increase of temperature leads to a lighter solution. An equation was formulated to correlate the experimental data. In this work, a nonlinear fitting was used to fit the viscosity values of pure 1DMA2P. All the results are shown in Figure 6. The figure shows that the nonlinear equation represents the experimental results well. The nonlinear equation used is shown as an Arrhenius relationship in Equation 7:

$$\text{Nonliner equation: } \eta = A \times \text{Exp}\left(\frac{B}{T}\right) \tag{7}$$

The values of the coefficients were obtained by fitting the experimental data to Equation (7). All the obtained coefficient results are shown in Equation (8):

$$\eta = 1.73 \times 10^{-3}\exp\left(\frac{1.96 \times 10^3}{T}\right) \tag{8}$$

TABLE 7 Coefficients of A_1, A_2, and A_3 for different concentration

Concentration (mol/L)	A_1	A_2	A_3
0.5	9.50E-05	−9.83E-05	−3.72E-04
1.0	2.09E-04	−2.06E-04	−4.02E-04
1.5	2.38E-04	−2.34E-04	−4.46E-04
2.0	3.29E-04	−2.62E-04	−5.30E-04
3.0	3.26E-04	−2.21E-04	−7.04E-04

TABLE 8 Coefficients of *B*

	B_1	B_2	B_3
A_1	−5.03E-05	2.69E-04	−2.42E-05
A_2	6.08E-05	−2.58E-04	8.25E-06
A_3	−3.35E-05	−1.73E-05	−3.53E-04

TABLE 6 Values of *A* for different concentration loaded 1-dimethylamino-2-propanol (1DMA2P) solution as function of CO_2 loading

0.5 mol/L		1.0 mol/L		1.5 mol/L		2.0 mol/L		3.0 mol/L	
CO_2 loading	*A*	CO_2 loading	*A*	CO_2 loading	*A*	CO_2 loading	*A*	CO_2 loading	*A*
0.05	−3.78E-04	0.07	−4.14E-04	0.07	−4.61E-04	0.08	−5.48E-04	0.08	−5.48E-04
0.14	−3.81E-04	0.12	−4.27E-04	0.17	−4.79E-04	0.15	−5.60E-04	0.15	−5.60E-04
0.25	−3.91E-04	0.25	−4.39E-04	0.28	−4.91E-04	0.18	−5.71E-04	0.18	−5.71E-04
0.35	−3.95E-04	0.33	−4.47E-04	0.37	−5.00E-04	0.33	−5.80E-04	0.33	−5.80E-04
0.45	−3.97E-04	0.40	−4.52E-04	0.45	−5.03E-04	0.39	−5.82E-04	0.39	−5.82E-04
0.59	−3.97E-04	0.49	−4.53E-04	0.52	−5.04E-04	0.52	−5.76E-04		
0.69	−3.94E-04	0.58	−4.51E-04	0.63	−4.98E-04	0.60	−5.70E-04		

The viscosity of unloaded 1DMA2P solution was measured over the concentration of 0.5–3 mol/L and the temperature range of 293–323 K. All the results are shown in Figure 7. As shown in the figure, the density exhibited a decreasing trend as the temperature for all different concentrations system was increased. This is consistent with the viscosity of liquids. From Figure 7, it can be seen that the viscosity decreased with an increase in the concentration at the same temperature. The more the molecules of 1DMA2P that are introduced into the system, the higher the viscosity of the 1DMA2P solution. The nonlinear equation (Equation 7) was used to correlate the experimental results as shown in Figure 7, which was observed to correlate the experimental viscosity data of 1DMA2P solution very well. All the coefficients of *A* and *B* of Equation (7) were obtained by using this nonlinear fitting. The results are shown in Table 10. The calculated results for viscosity were compared with the experimental results as shown in Figure 8. The figure shows that the predicated results have good agreement with the experimental data with an AAD of 2.5%.

In addition, the viscosity of 1DMA2P solution loaded with CO_2 was measured over the concentration of 0.5–3.0 mol/L and the temperature range of 293–323 K. All the results are shown in Figures S6–S10 in Supplemental Materials. From viscosity shown in Figures S6–S10, it was found that the viscosity of aqueous 1DMA2P solution changed as a function of CO_2 loading and temperature. As CO_2 loading increased, the viscosity only changed slightly for all concentrations. When CO_2 was injected into 1DMA2P solution, reactions of CO_2 with 1DMA2P occurred resulting in the production of ions (such as carbonates,

TABLE 9 Viscosity of the pure 1-dimethylamino-2-propanol (1DMA2P) over the temperature range of 20°C–50°C

Temperature (°C)	Dyn. viscosity (mPa·s)
20.00	1.410
25.00	1.248
30.00	1.115
35.00	1.003
40.00	0.907
45.00	0.826
50.00	0.756

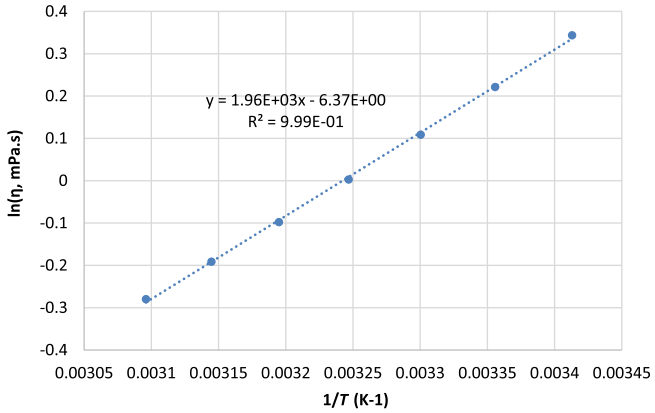

FIGURE 6 Effect of temperature on the viscosity of the pure 1-dimethylamino-2-propanol (1DMA2P)

TABLE 10 Coefficients of nonlinear equation for viscosity in unloaded 1-dimethylamino-2-propanol (1DMA2P) solution

Concentration (mol/L)	Coefficient of *A*	Coefficient of *B*
0.5	1.45E-04	2.72E+03
1.0	5.26E-04	2.37E+03
1.5	7.49E-05	3.05E+03
2.0	1.34E-04	2.92E+03
3.0	3.47E-05	3.46E+03

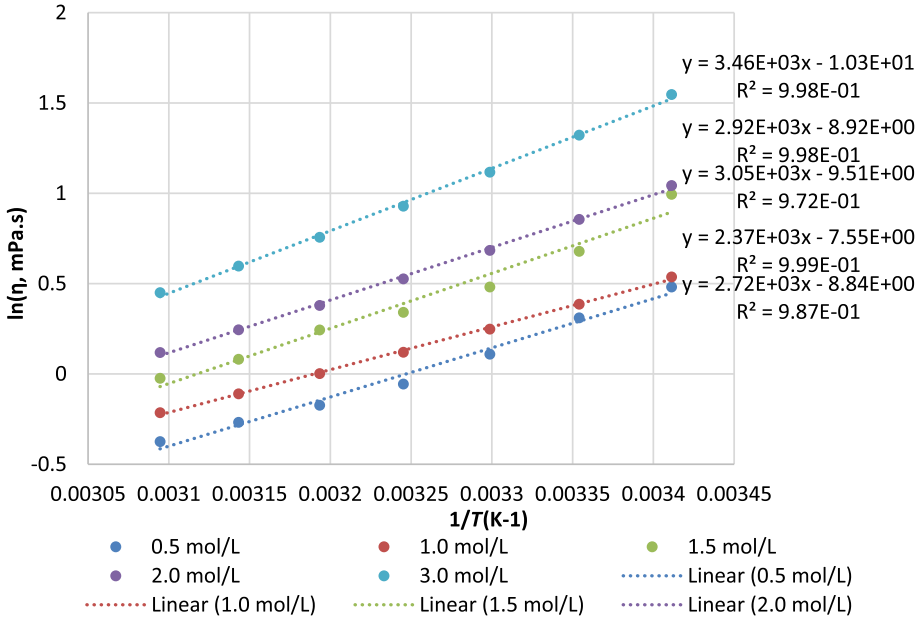

FIGURE 7 Viscosity of 1-dimethylamino-2-propanol (1DMA2P) solution at the concentration range of 0.5–3.0 mol/L and temperature range of 293–323 K

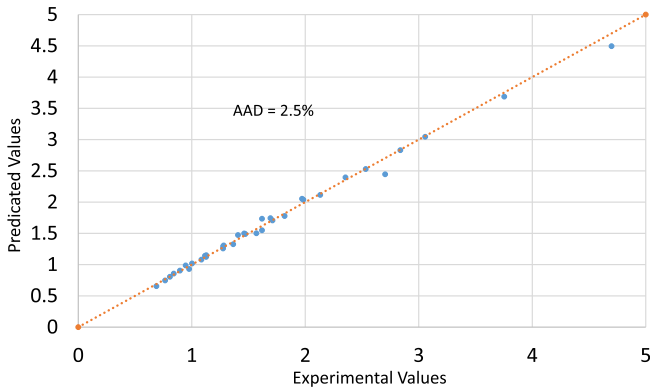

FIGURE 8 Parity plot of viscosity for the unloaded 1-dimethylamino-2-propanol (1DMA2P) solution of 0.5–3.0 mol/L and 293–323 K

bicarbonates, and protonated amine). However, the viscosity of 1DMA2P solution changed only slightly despite CO_2 loading increase. In order to represent the experimental viscosity data of loaded 1DMA2P solution, the equation proposed by Weiland et al.[27] was used to correlate the obtained values. This equation, which is considered as function of temperature, CO_2 loading, and amine concentration, could be expressed as:

$$\frac{\eta}{\eta_{H_2O}} = \exp\left(\frac{[(aw+b)\cdot T+(cw+d)]\cdot[\alpha(ew+fT+g)+1]\cdot w}{T^2}\right) \quad (9)$$

where η and η_{H_2O} are the viscosities of the amine solution and water, respectively, T is the temperature, w is the mass fraction.

The obtained viscosities of loaded 1DMA2P solution were correlated to Equation (9). The coefficients of a–f were estimated by fitting Equation (9) to the experimental viscosity data. All the results are shown in Table 11. The estimated coefficients of Equation (9) were used to represent the viscosity of the loaded 1DMA2P solution. It could be observed that the predicated results have good agreement with the experimental results with an AAD of 4.5%.

3.3 | Specific heat capacity

The specific heat capacity of pure 1DMA2P was measured over the temperature range of 298–323 K as shown in Figure 9. From this figure, it can be seen that the specific heat capacity increased as the temperature increased. For the correlation of the specific heat capacity of pure amine, a linear correlation was used to fit pure 2-amino-2-methyl-1-propanol and pure AEEA which were reported in the literature.[28,29] Linear fitting was used to fit the experimentally measured specific heat capacity values of pure 1DMA2P. All the results were shown in Figure 9. The figure shows that the linear equation represented the experimental results very well. The fitting linear equation is given in Equation (10):

TABLE 11 The parameters of correlations from Reference 27

Parameters	Values
a	4.34E-03
b	1.53E+01
c	2.90E+00
d	1.58E-06
e	1.16E-02
f	−1.01E-02
g	3.26E+00

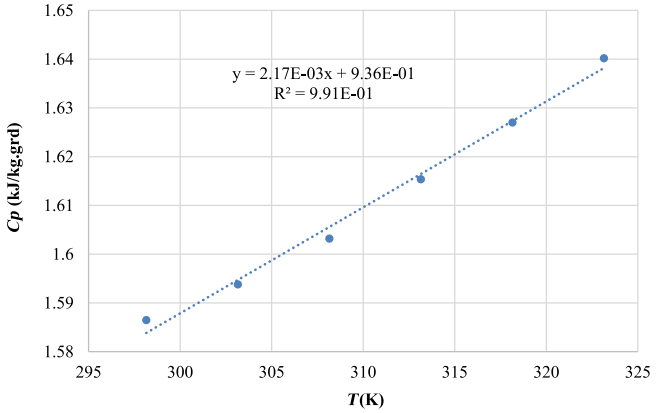

FIGURE 9 Specific heat capacity of pure 1-dimethylamino-2-propanol (1DMA2P) as function of temperature

$$Cp = 2.17\times10^{-3}\times T + 9.36\times10^{-1} \quad (10)$$

The specific heat capacity of unloaded 1DMA2P solution was measured over the concentration of 0.5–3 mol/L and the temperature range of 298–323 K. All the results are shown in Figure 10. In this figure, the specific heat capacity exhibited an increasing trend with an increase in temperature for all concentrations. It can also be seen in the figure that the specific heat capacity decreased with the increase in the concentration at the same temperature. This is because water has a higher specific heat capacity value than that 1DMA2P. In addition, the specific heat capacity of 1DMA2P solution with CO_2 loading were measured over the concentration of 0.5–3.0 mol/L and the temperature range of 298–323 K. These results are shown in Figures S11–S15 in Supplemental Materials. These figures show that the specific heat capacity of aqueous 1DMA2P solution changed as a function of CO_2 loading and temperature. Based on the figures for specific heat capacity of loaded 1DMA2P solution, the CO_2 loading had an effect on heat capacities for all concentrations. The introduction of CO_2 into 1DMA2P solution made the system to become complicated. The lower specific heat capacity of CO_2 in comparison with water and 1DMA2P reduced the value of the 1DMA2P-H_2O-CO_2. The Redlich–Kister equation, which could be considered to represent the excess molar specific heat capacity of amines, was used to correlate the experimental results as follows:

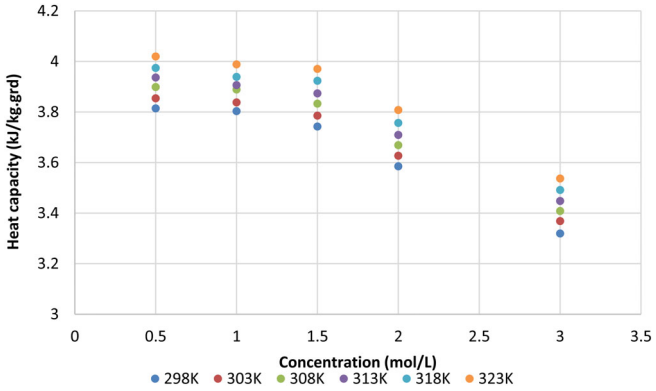

FIGURE 10 Specific heat capacity of unloaded 1-dimethylamino-2-propanol (1DMA2P) solution at the concentration of 0.5–3.0 mol/L and the temperature of 298–323 K

$$C_{P,12}^{E} = x_1 x_2 \sum_{i=0}^{n} A_i (x_1 - x_2)^i \tag{11}$$

where x_1 and x_2 are the mole fraction of component 1 and 2, respectively. A_i is a temperature dependence coefficient, which could be expressed as follows:

$$A_i = a_{i,0} + a_{i,1} \tag{12}$$

The excess molar heat capacities (C_P^E) were obtained by using the observed experimental molar specific heat capacity as in the following equation:

$$C_P^E = Cp - (x_1 Cp_1 + x_2 Cp_2) \tag{13}$$

It was found that the Redlich–Kister equation could correlate the experimental values very well with AAD of 3.5% and 4.2%, respectively.

3.4 | Analysis of physical properties of 1DMA2P using ANN models

3.4.1 | ANN model

ANN is an artificial intelligence method that mimics the human brain's operation and computation performance, and it has the ability to reflect the underlying linear or nonlinear relationships among input and target data.[30,31] Acquiring knowledge from an outside source, ANN stores information in its inner processing units and delivers them by means of the interaction of the transfer functions and the connection parameters between adjacent layers. An intact ANN is usually multiple-layered, and consists of one input layer, one output layer, and at least one hidden layer. A neuron is the basic structure unit of a network. Numerous neurons, which are distributed in different layers, are highly interconnected with others in adjacent layers, making up the configuration of a network. Multiple-layer networks with proper configuration are usually able to meet the requirement of the target processing system.[30] In this work, the back-propagation neural network (BPNN) model and basic description of radial basis function neural network (RBFNN) model were employed. The typical three-layer architectures of BPNN and RBFNN models are displayed in Figures 11 and 12, respectively. According to Rumelhart et al.,[32] BPNN model refers to a multilayer feed-forward network with a back-propagated learning process, which is based on the steepest gradient method and is considered to be one of the most widely used network architectures. The BPNN models used were established using the basic principles and working mechanisms. The following steps were followed[30]:

1. Data collection: Division of input/output data into training dataset and testing dataset.
2. Data normalization: All input data are normalized into [−1, 1].
3. Development of network configuration: The number of hidden layers, number of neurons of each layers, tanning algorithm, transfer functions, etc., are set up based on a trial and error method.
4. Information transfer: The processes of information from the input layer to hidden layers and then to output layers could be shown as the following equations: $A_3 = f_3(W_3 A_2 + B_3) = f_3(W_3(f_2(W_2 A_1 + B_2)) + B_3) = f_3(W_3(f_2(W_2(f_1(W_1 P + B_1)) + B_2)) + B_3)$
   where A_j, W_j, and B_j are the matrix of output values, weights and biases of the jth layer respectively, and fj is the transfer function ($j = 1$–3).
5. Error calculation: The errors of the output values and the experimental values are calculated. If the error is acceptable, the training is stopped. If not, the following steps have to be conducted.
6. Weights and biases adjustment: The weights and biases are adjusted based the following equations: $w_{k+1} = w_k + \gamma_k g_k$ and $b_{k+1} = b_k + \gamma_k g_k$. Where γ is learning rate, g is the momentum factor, and k is current training iteration.

Steps 4–6 run until the error is acceptable.

Basic description of RBFNN model is a feed-forward network that has been widely used in many research fields.[33,34] It is made up of three layers: one input layer, one output layer, and only one hidden layer. Each layer has its own neurons and connects with neurons in adjacent layer(s) in terms of weights (w), bias (b), and transfer functions to form the whole network structure. The most notable characteristic of RBFNN is its hidden layer transfer function between the input and the hidden layers, that is, the radial basis function (e.g., Gaussian function).

Similar to the BPNN, the process of development RBFNN consists of three parts: data collection, network structure modification, and parameter optimization.

3.4.2 | Analysis of density, viscosity, and specific heat capacity of 1DMA2P using ANN models

The ANN model can directly reflect and develop the linear or nonlinear relationship of the observed experimental data and the parameters, which can be considered to overcome the limitations of empirical

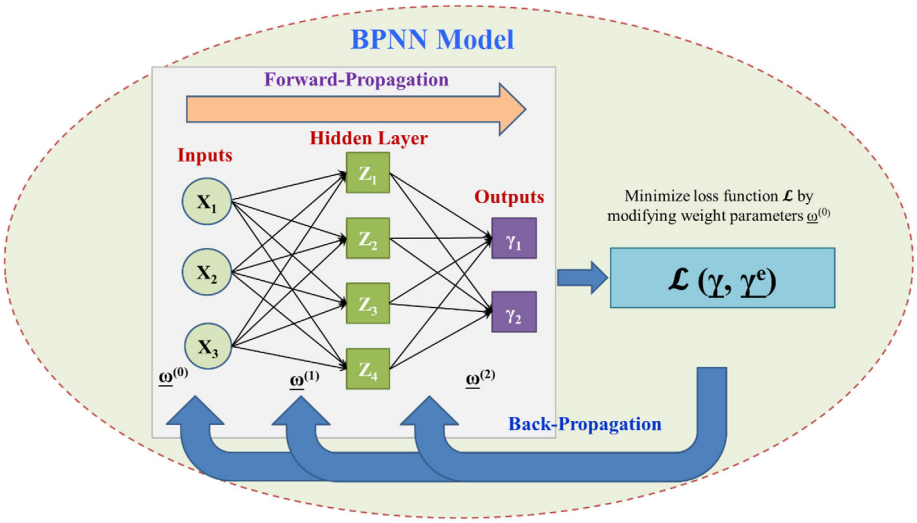

FIGURE 11 The basic structure of BPNN with multiple input parameters

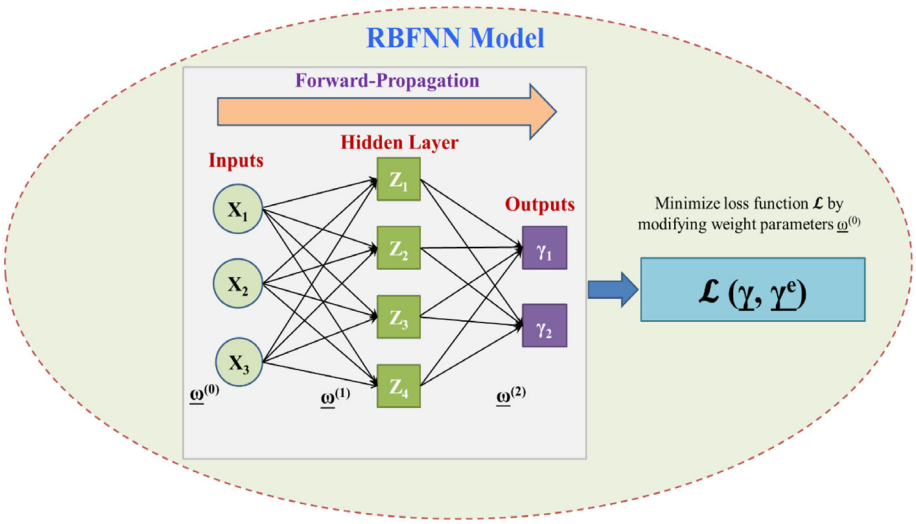

FIGURE 12 The basic structure of RBFNN with multiple input parameters

models (some assumptions in process of analysis experimental data).[30] The density, viscosity, and specific heat capacity of unloaded 1DMA2P solution and loaded 1DMA2P solution over the concentration of 0.5–3 mol/L and the temperature range of 293–323 K were analyzed using the trained BPNN and RBFNN models. The trained BPNN and RBFNN models were developed by using the 75% of the experimental data of density, viscosity, and specific heat capacity of 1DMA2P solution. Those selected experimental data of physical properties of 1DMA2P system were analyzed and predicted by the BPNN and RBFNN models. The predicted results were compared with their correlated experimental data in order to verify the effectiveness and accuracy of the BPNN and RBFNN models. The training effectiveness and accuracy of the BPNN and RBFNN models were evaluated by using the AAD. In order to achieve the trained BPNN and RBFNN models, the training process lasts until the training effectiveness and accuracy reached an acceptable level.

The training results in terms of AADs are shown in Table 12. The table shows that the trained BPNN and RBFNN models for the density of unloaded 1DMA2P solution were trained very well with the AADs of 0.03% and 0.02%, respectively. The trained BPNN and RBFNN models for the density of loaded 1DMA2P solution were trained very well with the AADs of 0.09% and 0.04%, respectively. All those results showed that the well-trained BPNN and RBFNN models could be used to predicate the density of loaded and unloaded 1DMA2P solution. By using the developed BPNN and RBFNN models, the rest (25%) of the experimental density of unloaded 1DMA2P solution and loaded 1DMA2P solution were predicted. All the predicated results are shown and compared with the experimental results. These are presented in Figures S16–S19 in Supplemental Materials. As shown in these figures, it can be seen that the trained BRNN and RBFNN models could represent the density of unloaded 1DMA2P solution very well with ADDs of 0.09% and 0.12%, respectively. As well, those two trained models represented the density of loaded 1DMA2P solution very well with AADs of 0.09% for BPNN and 0.01% for RBFNN, respectively.

TABLE 12 AADs performance of trained models

	Density		Viscosity		Specific heat capacity	
	BPNN	RBFNN	BPNN	RBFNN	BPNN	RBFNN
Unloaded 1DMA2P	0.03%	0.02%	2.66%	1.05%	0.04%	0.07%
Loaded 1DMA2P	0.09%	0.04%	3.24%	1.53%	0.20%	0.51%

Abbreviations: 1DMA2P, 1-dimethylamino-2-propanol; AAD, absolute average deviation; BPNN, back-propagation neural network; RBFNN, radial basis function neural network.

In addition, the trained model for representation viscosity was also developed in this work as well. As shown in Table 12, it could be seen that the BPNN and RBFNN models for unloaded 1DMA2P solution and loaded 1DMA2P solution were trained very well. As shown in Table 12, ADDs of trained BPNN model were 2.66% for unloaded 1DMA2P solution and 3.24% for loaded 1DMA2P solution, respectively. The ADDs of trained RBFNN model were 1.05% for unloaded 1DMA2P solution and 1.53% for loaded 1DMA2P solution, respectively. As those models were well-trained, all of them were used to represent the rest of the experimental data for viscosity. All the predicted results were plotted against the experimental results, which are shown in Figures S20–S23 in Supplemental Materials. As shown in Figures S20 and S21, the BPNN and RBFNN models provided good prediction for the viscosity of unloaded 1DMA2P solution with AADs of 3.5% and 5.4%, respectively. Also, as shown in Figures S22 and S23, the BPNN and RBFNN models provided good prediction for viscosity of loaded 1DMA2P solution with AADs of 3.2% and 2.5%, respectively.

For the specific heat capacity data, the BPNN model and RBFNN model were also well trained. All the results are presented in Table 12. From Table 12, the ADDs of BPNN model for unloaded 1DMA2P solution and loaded 1DMA2P solution were observed to be 0.04% and 0.20%, respectively. The ADDs of RBFNN model for unloaded 1DMA2P solution and loaded 1DMA2P solution were 0.07% and 0.51%, respectively. From the results shown in Table 12, it can be concluded that those models were well trained and could be used to represent the remaining experimental results. All the predicted results were plotted against the experimental results, as shown in Figures S24–S27 in Supplemental Materials. As shown in Figures S24 and S25, the BPNN model and RBFNN models provided good prediction for the specific heat capacity of the unloaded 1DMA2P solutions with AADs of 0.61% and 0.44%, respectively. Also, as shown in Figures S26 and S27, the BPNN model and RBFNN model provided good prediction for the specific heat capacity of loaded 1DMA2P solution with AADs of 3.2% and 2.5%, respectively.

As shown earlier, the developed ANN models (BPNN and RBFNN) in this present work could represent the experimental physical properties of 1DMA2P very well and also could be used to provide accurate data for physical properties of 1DMA2P without conducting many experiments. However, it should be noted that those models could only be used to predict the unknown CO_2 solubility based on experimental conditions of the physical properties for 1DMA2P. Even though the ANN is an effective, convenient, and practical technique, the disadvantage of ANN is that ANN could not elucidate the relationship between input parameters and output values. Thus, the trained ANN models cannot be applied beyond the conditions of the experimental data, which were used to train the model.

3.5 | Comparison of empirical models and ANN models

In this work, empirical and ANN models for prediction of physical properties of 1DMA2P were developed and used to represent the experimental results. The performance of the empirical and ANN models for prediction of physical properties was given in terms of ADDs, which were shown in Table 13. It can be seen that both the empirical models and ANN models could predict the physical properties in 1DMA2P solution. Empirical models gave good performance in the prediction of density, viscosity, and specific heat capacity. ANN models (BPNN model and RBFNN model) resulted in a lower AAD than most of the empirical models. With respect to the accurate predication, ANN models certainly performed better. However, the limitation of ANN models is that it cannot reflect the relationship between input parameters and output values. Thus, it could only be used to predict the physical properties based on experimental conditions of the physical properties. Empirical models were developed based on a certain relationship of input parameters and output data. Same as ANN models, empirical models may not be expanded across the experimental conditions. All in all, a well-trained ANN model is an efficiently accurate method to represent the data located within the experimental conditions.

Thus, ANN models could be considered as one method to provide accurate physical properties of amines. Also, developed ANN models obtained in this present work could provide an accurate data for CO_2 equilibrium solubility without conducting many experiments. Even though the ANN method is an effective, convenient, and practical technique, the disadvantage is that ANN could not elucidate the relationship between input parameters and output values. Those models could only be used to predicate the unknown physical properties located into experimental conditions of the physical properties for 1DMA2P due to the derivation process. All in all, the trained ANN models cannot be applied beyond the condition of experimental data which were used to train the model. ANN models with a relationship of inputs and outputs should be further addressed in order to reasonably represent the experimental results, which deserved more efforts.

TABLE 13 Comparison of empirical model and ANN model in terms of AADs

	Density			Viscosity			Specific heat capacity		
	EM	BPNN	RBFNN	EM	BPNN	RBFNN	EM	BPNN	RBFNN
Unloaded 1DMA2P	2.3%	0.09%	0.12%	2.5%	3.6%	5.4%	3.5%	0.63%	0.44%
Loaded 1DMA2P	4.05%	0.09%	0.11%	4.5%	3.2%	2.5%	4.2%	0.65%	0.93%

Abbreviations: 1DMA2P, 1-dimethylamino-2-propanol; AAD, absolute average deviation; BPNN, back-propagation neural network; EM, empirical model; RBFNN, radial basis function neural network.

4 | CONCLUSIONS

In this work, densities, viscosities of pure 1DMA2P, unloaded 1DMA2P solution, and loaded 1DMA2P solution were measured over the 1DMA2P concentration range of 0.5–3.0 mol/L, temperature range of 293–323 K. The results of pure 1DMA2P gave a decreasing trend as the temperature was increased. The results of unloaded 1DMAP solution and loaded 1DMA2P solution showed that the densities and viscosities of unloaded 1DMA2P decreased with an increase of 1DMA2P concentration and temperature. Based on the results for loaded 1DMA2P solution, the addition of CO_2 has some effect on density and viscosity of the solution.

The specific heat capacity of pure 1DMA2P, unloaded 1DMA2P solution, and loaded 1DMA2P solution were also measured at the concentration of 0.5–3.0 mol/L and temperature range of 298–323 K. In order to correlate the obtained results, some empirical models were employed to represent the experimental physical properties of 1DMA2P. Those models show good prediction of the physical properties with acceptable ADDs. In addition, ANNs models (BPNN and RBFNN model) were developed and used to correlate the physical properties of 1DMA2P. The obtained BPNN and RBFNN models could correlate the experimental results very well. A comparison of ANN models and empirical models indicated that the well-trained ANN models could be considered as an efficient and accurate method to represent the data located within the experimental conditions for use of the physical properties. ANN models with a relationship of inputs and outputs should be further addressed in order to reasonably represent the experimental results.

AUTHOR CONTRIBUTIONS

Helei Liu: Conceptualization (equal); data curation (lead); formal analysis (lead); investigation (lead); methodology (equal); supervision (equal); writing – original draft (equal). **Xiaotong Jiang:** Data curation (supporting); formal analysis (supporting); investigation (supporting); methodology (supporting); validation (lead); writing – original draft (equal); writing – review and editing (supporting). **Raphael Idem:** Conceptualization (equal); funding acquisition (equal); project administration (equal); resources (lead); supervision (lead); writing – review and editing (equal). **Shoulong Dong:** Conceptualization (equal); formal analysis (supporting); writing – review and editing (equal). **Paitoon Tontiwachwuthikul:** Funding acquisition (equal); project administration (equal); resources (equal); supervision (supporting).

ACKNOWLEDGMENTS

The financial support by the Natural Science and Engineering Research Council of Canada (NSERC), and financial support from talent project from Beijing Institute of Technology (2022CX01004) is gratefully acknowledged.

DATA AVAILABILITY STATEMENT

Data derived from public domain resources.

ORCID

Helei Liu https://orcid.org/0000-0002-8230-5865
Raphael Idem https://orcid.org/0000-0002-2708-0608
Shoulong Dong https://orcid.org/0000-0002-4956-4160
Paitoon Tontiwachwuthikul https://orcid.org/0000-0003-0187-3420

REFERENCES

1. Matthews A. Are the COP26 climate change negotiations ready to embrace agriculture? *EuroChoices*. 2021;20(2):4-10.
2. Carrera E, Azzaro-Pantel C. Bi-objective optimal design of hydrogen and methane supply chains based on power-to-gas systems. *Chem Eng Sci*. 2021;246:116861.
3. Terlouw T, Treyer K, Bauer C, Mazzotti M. Life cycle assessment of direct air carbon capture and storage with low-carbon energy sources. *Environ Sci Technol*. 2021;55(16):11397-11411.
4. Ai Z, Hanasaki N, Heck V, Hasegawa T, Fujimori S. Global bioenergy with carbon capture and storage potential is largely constrained by sustainable irrigation. *Nat Sustain*. 2021;4:1-8.
5. Basile A, Gugliuzza A, Iulianelli A, Morrone P. Membrane technology for carbon dioxide (CO_2) capture in power plants. *Advanced Membrane Science and Technology for Sustainable Energy and Environmental Applications*. Elsevier; 2011:113-159.
6. Zamarripa MA, Eslick JC, Matuszewski MS, Miller DC. Multi-objective optimization of membrane-based CO_2 capture. *Comput Aided Chem Eng*. 2018;44:1117-1122.
7. Jongpitisub A, Siemanond K, Henni A. Simulation of carbon-dioxide-capture process using aqueous ammonia. *Comput Aided Chem Eng*. 2015;37:1301-1306.
8. Gruenewald M, Radnjanski A. Gas–liquid contactors in liquid absorbent-based PCC. *Absorption-Based Post-Combustion Capture of Carbon Dioxide*. Elsevier; 2016:341-363.
9. Moioli S, Pellegrini LA. Modeling the methyldiethanolamine-piperazine scrubbing system for CO_2 removal: thermodynamic analysis. *Front Chem Sci Eng*. 2016;10(1):162-175.
10. Wanderley RR, Yuan Y, Rochelle GT, Knuutila HK. CO_2 solubility and mass transfer in water-lean solvents. *Chem Eng Sci*. 2019;202:403-416.

11. Sanchez-Fernandez E, Heffernan K, Van Der Ham L, et al. Analysis of process configurations for CO_2 capture by precipitating amino acid solvents. *Ind Eng Chem Res*. 2014;53(6):2348-2361.
12. Moioli S, Pellegrini LA, Ho MT, Wiley DE. A comparison between amino acid based solvent and traditional amine solvent processes for CO_2 removal. *Chem Eng Res Design*. 2019;146:509-517.
13. Li K, Leigh W, Feron P, Yu H, Tade M. Systematic study of aqueous monoethanolamine (MEA)-based CO_2 capture process: techno-economic assessment of the MEA process and its improvements. *Appl Energy*. 2016;165:648-659.
14. Luo W, Yang Q, Conway W, Puxty G, Feron P, Chen J. Evaluation and modeling of vapor–liquid equilibrium and CO_2 absorption enthalpies of aqueous designer diamines for post combustion capture processes. *Environ Sci Technol*. 2017;51(12):7169-7177.
15. Yu B, Yu H, Li K, et al. Characterisation and kinetic study of carbon dioxide absorption by an aqueous diamine solution. *Appl Energy*. 2017;208:1308-1317.
16. Zheng W, Xiao M, Liu H, Gao H, Liang Z. Modeling and experiments of equilibrium solubility of carbon dioxide in aqueous N-(2-hydroxyethyl) pyrrolidine solution. *J Taiwan Inst Chem Eng*. 2018;85:132-140.
17. Kadiwala S, Rayer AV, Henni A. Kinetics of carbon dioxide (CO_2) with ethylenediamine, 3-amino-1-propanol in methanol and ethanol, and with 1-dimethylamino-2-propanol and 3-dimethylamino-1-propanol in water using stopped-flow technique. *Chem Eng J*. 2012;179:262-271.
18. Chowdhury FA, Yamada H, Higashii T, Goto K, Onoda M. CO_2 capture by tertiary amine absorbents: a performance comparison study. *Ind Eng Chem Res*. 2013;52(24):8323-8331.
19. Liang Y, Liu H, Rongwong W, Liang Z, Idem R, Tontiwachwuthikul P. Solubility, absorption heat and mass transfer studies of CO_2 absorption into aqueous solution of 1-dimethylamino-2-propanol. *Fuel*. 2015;144:121-129.
20. Liu H, Gao H, Idem R, Tontiwachwuthikul P, Liang Z. Analysis of CO_2 solubility and absorption heat into 1-dimethylamino-2-propanol solution. *Chem Eng Sci*. 2017;170:3-15.
21. Liu H, Idem R, Tontiwachwuthikul P. Novel models for correlation of solubility constant and diffusivity of N_2O in aqueous 1-dimethylamino-2-propanol. *Chem Eng Sci*. 2019;203:86-103.
22. Park J-Y, Yoon SJ, Lee H, et al. Density, viscosity, and solubility of CO_2 in aqueous solutions of 2-Amino-2-hydroxymethyl-1, 3-propanediol. *J Chem Eng Data*. 2002;47(4):970-973.
23. Eckert J. Selecting proper distillation column packing. *Chem Eng Prog*. 1970;66(3):39.
24. Wang G, Yuan X, Yu K. Review of mass-transfer correlations for packed columns*. *Ind Eng Chem Res*. 2005;44(23):8715-8729.
25. Gao H, Gao G, Liu H, Luo X, Liang Z, Idem RO. Density, viscosity, and refractive index of aqueous CO_2-loaded and-unloaded ethylaminoethanol (EAE) solutions from 293.15 to 323.15 K for post combustion CO_2 capture. *J Chem Eng Data*. 2017;62(12):4205-4214.
26. Hartono A, Svendsen HF. Density, viscosity, and excess properties of aqueous solution of diethylenetriamine (DETA). *J Chem Thermodyn*. 2009;41(9):973-979.
27. Weiland RH, Dingman JC, Cronin DB, Browning GJ. Density and viscosity of some partially carbonated aqueous alkanolamine solutions and their blends. *J Chem Eng Data*. 1998;43(3):378-382.
28. Mathonat C, Maham Y, Mather AE, Hepler LG. Excess molar enthalpies of (water+ monoalkanolamine) mixtures at 298.15 K and 308.15 K. *J Chem Eng Data*. 1997;42(5):993-995.
29. Mundhwa M, Henni A. Molar heat capacity of various aqueous alkanolamine solutions from 303.15 K to 353.15 K. *J Chem Eng Data*. 2007;52(2):491-498.
30. Chen G, Luo X, Zhang H, et al. Artificial neural network models for the prediction of CO_2 solubility in aqueous amine solutions. *Int J Greenh Gas Control*. 2015;39:174-184.
31. Chan V, Chan C. Learning from a carbon dioxide capture system dataset: Application of the piecewise neural network algorithm. *Petroleum*. 2017;3(1):56-67.
32. Rumelhart DE, Hinton GE, Williams RJ. Learning representations by back-propagating errors. *Nature*. 1986;323:533-538.
33. Beatson RK, Newsam GN. Fast evaluation of radial basis functions: I. *Comput Math Appl*. 1992;24(12):7-19.
34. Fu K, Chen G, Liang Z, Sema T, Idem R, Tontiwachwuthikul P. Analysis of mass transfer performance of monoethanolamine-based CO_2 absorption in a packed column using artificial neural networks. *Ind Eng Chem Res*. 2014;53(11):4413-4423.

SUPPORTING INFORMATION

Additional supporting information may be found in the online version of the article at the publisher's website.

How to cite this article: Liu H, Jiang X, Idem R, Dong S, Tontiwachwuthikul P. AI models for correlation of physical properties in system of 1DMA2P-CO_2-H_2O. *AIChE J*. 2022;68(9):e17761. doi:10.1002/aic.17761